

Defect-induced spatial coherence in the discrete nonlinear Schrödinger equationC. L. Pando L.¹ and E. J. Doedel²¹*IFUAP, Universidad Autónoma de Puebla, Apartado Postal J-48, Puebla, Puebla 72570, Mexico*²*1455 Boulevard de Maisonneuve West, Montreal, Quebec H3G 1M8, Canada*

(Received 21 July 2003; published 22 March 2004)

We have considered the discrete nonlinear Schrödinger equation (DNLSE) with periodic boundary conditions in the context of coupled Kerr waveguides. The presence of a defect in the central oscillator equation can induce quasiperiodic or large chaotic amplitude oscillations. As for the quasiperiodic dynamics, an enhancement of the amplitude correlations in certain oscillator pairs can take place. However, when the array dynamics becomes chaotic, these correlations are destroyed, and, for suitable defects, synchronization, in the information sense, of certain signals arises in this Hamiltonian system. A numerical continuation analysis clarifies the onset of this dynamical regime. In this case, phase synchronization follows with a peculiar distribution of the Liapunov exponents. These effects occur for initial conditions in a small neighborhood of a family of stationary solutions. We have also found a regime characterized by persistent localized chaotic amplitudes. We have generalized these results to take into account birefringent effects in waveguides.

DOI: 10.1103/PhysRevE.69.036603

PACS number(s): 42.65.Tg, 05.45.-a, 87.10.+e

I. INTRODUCTION

Nonlinear effects in waveguide arrays have been studied intensively in the past several years, both theoretically [1,2] and experimentally [3–5]. The propagation of waves in these arrays is associated with new and interesting effects not reflected in continuous media [1,2]. By injecting a strong optical field, certain field distributions propagate while keeping a fixed spatial profile in a limited number of Kerr waveguides. These stationary fields are known as discrete spatial solitons (DSS's) or breathers [6]. In nonlinear optics, the existence of DSS's was theoretically predicted for the first time in Ref. [1]. The differences with the continuous system become clear if the DSS are forced to move across the array. In this case, these DSS tend to propagate along the waveguides. The equation that describes these waveguide arrays is referred to as the discrete nonlinear Schrödinger equation (DNLSE). In contrast, the continuum limit of the DNLSE is translationally invariant [2,5]. Recently, a comprehensive review on the DNLSE was published in Ref. [7]. The DNLSE describes, among other systems, localized modes in long protein systems [8] and arrays of nonlinear mechanical pendula [9]. The theoretical predictions of the DSS have been verified recently in experimental observations in Kerr waveguide arrays [3,4,10] typically using $\text{Al}_x\text{Ga}_{1-x}\text{As}$ as Kerr media. Several types of defects in planar waveguide arrays were studied experimentally in Ref. [11]. As for applications, recently a model describing diffraction managed nonlinear waveguide arrays has been reported [12] which supports modulated DSS as well as chaotic solutions. The DNLSE also arises in models of Bose-Einstein condensates (BEC's) trapped in periodic potentials generated by optical standing waves [13]. Indeed, the dynamics of this BEC is governed by the Gross-Pitaevskii equation and can be mapped, in the tight binding approximation, to a DNLSE [13].

In this work, we study a family of solutions of the DNLSE with periodic boundary conditions and on-site defects. Small defects induce relevant bifurcations and interest-

ing behavior in these new solutions. Moreover, we study the intensity correlations of the electromagnetic fields that arise in certain pairs of waveguides when the system dynamics is quasiperiodic or chaotic. In this Hamiltonian system, we show that it is possible to synchronize, in the information sense, certain chaotic signals generated by different waveguide pairs. Based on an information theory approach, chaos synchronization has been considered recently in experimental time series and theoretical models [14,15]. We have found special properties in these solutions using order parameters, Liapunov exponents, and phase locking features. This article has seven sections. The DNLSE is discussed in Sec. II in the framework of nonlinear optics. A family of stationary solutions is discussed in Sec. III. In Sec. IV, the quasiperiodic regime of these solutions induced by a defect is considered. In Sec. V, we discuss the chaotic case of this system. In Sec. VI, we consider a generalization of these solutions in a DNLSE that takes into account elliptical birefringence in waveguides. Finally, in Sec. VII we give the conclusions.

II. THE MODEL

We consider an array of one-dimensional coupled waveguides. The neighboring waveguides are separated from each other by the same distance d and therefore the coupling constant between these is the same. We consider the case with no losses and continuous excitation. Within the framework of the coupled mode theory, the evolution of E_n , the electric field envelope in the n th waveguide, is given by the following equation [2]:

$$i \frac{\partial E_n}{\partial z} + \beta_n E_n + C(E_{n-1} + E_{n+1}) + \gamma |E_n|^2 E_n = 0. \quad (1)$$

This system is assumed to have periodic boundary conditions. In Eq. (1), β_n is the linear propagation constant of each waveguide, C is the linear coupling coefficient, and γ is the nonlinear parameter. By introducing the dimensionless field

$Q_n = \sqrt{\gamma/2CE_n} \exp[-i(\beta+2C)z]$, Eq. (1) transforms into the discrete nonlinear Schrödinger equation given by

$$i \frac{\partial Q_n}{\partial \zeta} + \delta_n Q_n + (Q_{n-1} + Q_{n+1} - 2Q_n) + 2|Q_n|^2 Q_n = 0, \quad (2)$$

where $\zeta = Cz$ is the normalized propagation distance and $\delta_n = (\beta_n - \beta)/C$. The Hamiltonian equations related to the DNLS equation can be obtained by transforming into action-angle variables (I_n, θ_n) , where $Q_n = \sqrt{I_n} \exp(-i\theta_n)$. The quantity $I_n \equiv P_n^2$ stands for the light intensity of the n th waveguide [7]. The equations for P_n and θ_n are the following:

$$\begin{aligned} \frac{dP_n}{d\zeta} &= P_{n-1} \sin(\theta_{n-1} - \theta_n) + P_{n+1} \sin(\theta_{n+1} - \theta_n), \\ \frac{d\theta_n}{d\zeta} &= 2 - \delta_n - \frac{P_{n-1} \cos(\theta_{n-1} - \theta_n)}{P_n} \\ &\quad - \frac{P_{n+1} \cos(\theta_{n+1} - \theta_n)}{P_n} - 2P_n^2. \end{aligned} \quad (3)$$

III. NEW STATIONARY SOLUTIONS AND THEIR STABILITY

We will consider two examples of a family of DNLS stationary solutions. These solutions depend harmonically on ζ . To find these, we deal with the nonlinear map approach [16,17]. We underline that there are different ways to find stationary solutions of the DNLS equation [7], one of which relies on the solution of a set of nonlinear algebraic equations for a given coupling constant and then makes use of continuation methods [7]. In Ref. [16], it was shown that homoclinic and heteroclinic orbits of a suitable Hamiltonian map support breather solutions in the DNLS equation. Instead, we will consider those DNLS stationary solutions which are determined by the (elliptic) stable periodic orbits of the Hamiltonian map mentioned above. These two types of DNLS solutions are clearly different. Indeed, these elliptic and homoclinic orbits, as is well known, have different origins and properties [18]. While the first are periodic, according to the Poincaré-Birkhoff theorem, the homoclinic orbits have no periodicity, i.e., repeated iteration of the associated map produces new homoclinic points [18]. These new solutions are obtained by making $dP_n/d\zeta = 0$ and $\theta_n = \theta_m$ for any $n \neq m$. Moreover, we can define the frequencies on the tori $I_n = P_n^2$ by setting $d\theta_n/d\zeta = \lambda$, where λ is a constant. Therefore, the stationary solutions have the form $Q_n(\zeta) = P_n \exp(-i\lambda\zeta)$. As a result, the following map is obtained:

$$\begin{aligned} X_{n+1} &= P_n, \\ P_{n+1} &= (\Gamma_n - 2|P_n|^2)P_n - X_n, \end{aligned} \quad (4)$$

where $\Gamma_n = 2 - \lambda - \delta_n$. The Jacobian J of this map is area preserving, i.e., $J = 1$. We will consider in this section the case $\Gamma = 2 - \lambda$ for which $\delta_n = 0$. For the sake of definition, we will label Eq. (4) as the cubic map (CM). This map has the symmetry $X_n \rightarrow -X_n$ and $P_n \rightarrow -P_n$. The fixed points of the

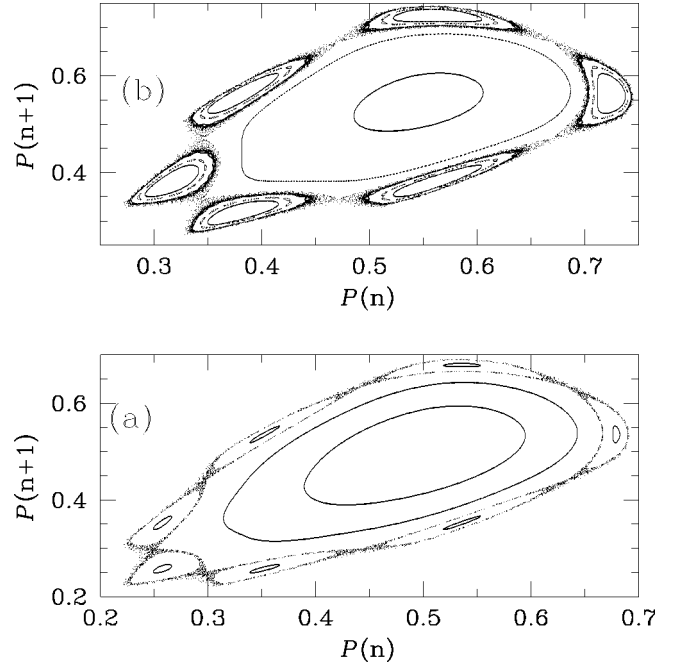


FIG. 1. Plot of the stationary field P_n versus P_{n+1} for (a) $\Gamma = 2.5$ and (b) $\Gamma = 2.6$.

CM are $(0,0)$ and $(\pm\sqrt{\Gamma/2-1}, \pm\sqrt{\Gamma/2-1})$. After considering the linearization of the CM, it is found that the point $(0,0)$ is elliptic for $|\Gamma| < 2$, for $\Gamma = 2$, it is parabolic and finally for $\Gamma > 2$, it becomes a saddle point. Instead, the fixed points $(\pm\sqrt{\Gamma/2-1}, \pm\sqrt{\Gamma/2-1})$ are elliptic for $2 < \Gamma < 4$, for $\Gamma = 4$, these are parabolic and finally for $\Gamma > 4$, both points become saddle points. Now, we proceed to illustrate the presence of resonances and island chains localized around the elliptic points. When $\Gamma = 2.5$, we find a saddle point at $(0,0)$ and two elliptic points at $(\pm\sqrt{\Gamma/2-1}, \pm\sqrt{\Gamma/2-1})$. In Fig. 1(a), quasiperiodic orbits surround the elliptic point $(\sqrt{\Gamma/2-1}, \sqrt{\Gamma/2-1})$ and further away, we identify a period seven island chain and its resonances. Surrounding these resonances, we also observe the characteristic chaotic sea [18]. When $\Gamma = 2.6$, $(0,0)$ is a saddle point while $(\pm\sqrt{\Gamma/2-1}, \pm\sqrt{\Gamma/2-1})$ are elliptic points. In Fig. 1(b), surrounding the elliptic point $(\sqrt{\Gamma/2-1}, \sqrt{\Gamma/2-1})$, we find an island chain of period 6. We will show that the resonances of period $M = 6$ and $M = 7$ generate stable stationary DNLS solutions in a ring of M coupled waveguides. These two stationary solutions P_n are shown in Fig. 2. The stability of these solutions P_n was numerically studied by integrating the DNLS equation. We have carried out these integrations with slightly different initial conditions [19]. That is, $Q_n(\zeta = 0) = P_n + \nu_n$, where ν_n stands for a small random perturbation. In addition, we have considered the Liapunov exponents of the corresponding linearized equations [18]. We have found numerically that our stationary solutions are stable since all the Liapunov exponents Λ_n of this system converge towards zero.

We underline that the parameter λ is relevant to find the resonance under consideration in the CM of Eq. (4) and, therefore, λ parametrizes the actions $I_n = P_n^2$. We also

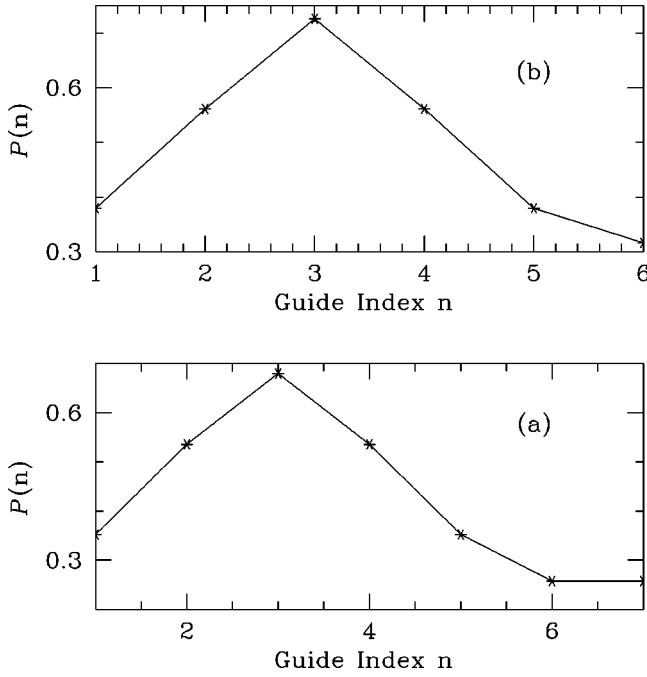


FIG. 2. Plot of the stationary field amplitudes P_n versus waveguide index n . (a) Period seven resonance and $\Gamma=2.5$ and (b) period six resonance and $\Gamma=2.6$.

have observed that our DNLSE solutions are robust with respect to perturbations of the kind $|Q_n|^{2\sigma}Q_n$, where $\sigma \approx 1$. The DNLSE stationary solution, which is generated by the resonance of period 7 around the elliptic point $[(-\lambda/2)^{1/2\sigma}(-\lambda/2)^{1/2\sigma}]$ in the associated map, is still stable. The map eigenvalues of this equilibrium point are given by $1 + \sigma\lambda \pm \sqrt{\lambda^2\sigma^2 + 2\lambda\sigma}$. This more general equation is known as the generalized DNLSE (GDNLSE) [7]. We note that the elliptic points of the CM were considered as standing wave solutions of a DNLSE consisting of a large number of oscillators [20]. In our solutions, instead, the number of oscillators, i.e., waveguides, coincides with the period of the map resonance and, moreover, the phases of the oscillators differ by a small perturbation, i.e., these are phase locked.

IV. QUASIPERIODIC SOLUTIONS

In this section, we add a defect to the linear propagation constant of the central waveguide and consider the quasiperiodic solutions of this system. That is, we study the case where $\delta_3 > 0$ and $\delta_n = 0$ for $n \neq 0$. The central waveguide, in both Figs. 2(a) and 2(b), has precisely the largest intensity. We make use of the stationary DNLSE solutions of the previous section as initial conditions for this perturbed DNLSE. This defect induces correlations between the intensities of a given pair of waveguides. We consider the linear correlation function R to estimate the level of association between these intensities. The intensities of the waveguides i and j are fully correlated (uncorrelated) when $R=1$ ($R=0$), where

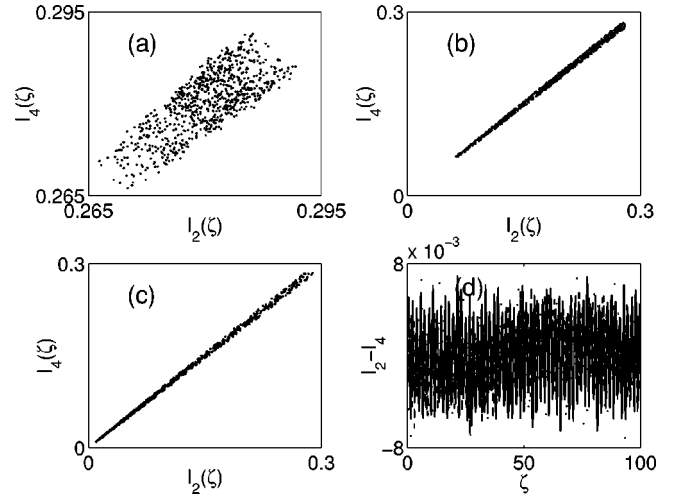


FIG. 3. Plot of $I_2(\zeta)$ versus $I_4(\zeta)$ for (a) $\delta_3=0.025$, (b) $\delta_3=0.4$, and (c) $\delta_3=1.25$. (a) Plot of $I_4 - I_2$ versus ζ for $\delta_3=0.025$ (solid line), $\delta_3=0.4$ (dashed line), and $\delta_3=1.25$ (dotted line).

$$R = \frac{\sum_{i=1}^N [I_j(i) - \langle I_j \rangle][I_k(i) - \langle I_k \rangle]}{\sqrt{\sum_{i=1}^N [I_j(i) - \langle I_j \rangle]^2} \sqrt{\sum_{i=1}^N [I_k(i) - \langle I_k \rangle]^2}}$$

and $\langle \dots \rangle$ stands for spatial average. The significance level of R in our calculations is good enough. The intensities of the second and fourth waveguides have the least degree of correlation among all waveguide pairs. For $\delta_3=0.025$, Fig. 3(a) shows that I_2 and I_4 have a slight correlation but still their oscillation amplitudes are similar to the maximum of $|I_2 - I_4|$.

Instead, when $\delta_3=0.4$ and $\delta=1.25$, as observed in Figs. 3(b) and 3(c), respectively, the intensities I_2 and I_4 have increased largely their degree of correlation. In these figures, the magnitude of the intensity oscillations has increased more than 10 times with respect to the case when $\delta_3=0.025$. However, as shown in Fig. 3(d), the boundaries of the difference $\Delta I = |I_2 - I_4|$ remain basically unchanged as the defect δ_3 takes on different values. As long as the dynamics is quasiperiodic, this explains why $R \rightarrow 1$ as δ_3 increases.

To qualitatively understand the linear correlation growth $R \rightarrow 1$ as δ_3 increases, it is enough to consider a simplified model consisting of three waveguides Q_{-1} , Q_0 , and Q_1 , where $Q_{-1} \approx Q_1$, $|\delta_0| \ll 1$, and $\delta_1 = \delta_{-1} = 0$. This simplified model explains, on the one hand, the enhancement of the oscillation amplitudes of $Q_{-1} \approx Q_1$ and, on the other hand, the stability of the small oscillations of $\theta_1 - \theta_{-1}$ and $|Q_{-1}| - |Q_1|$, which on average vanish. This agrees with the typical behavior of symmetric waveguides such as Q_2 and Q_4 . Thus, the system for the three modes takes the form

$$i \frac{dQ_0}{d\zeta} + \delta_0 Q_0 + 2|Q_0|^2 Q_0 + 2Q_1 = 0,$$

$$i\frac{dQ_1}{d\zeta} + 2|Q_1|^2Q_1 + Q_0 + Q_1 = 0, \quad (5)$$

where the labels are the same as in Eq. (2) and $\delta_0 = (\beta_0 - \beta_1)/C$. To explain the enhancement of the oscillation amplitudes of Q_0 and Q_1 , we have imposed the symmetry relation $Q_1 = Q_{-1}$. By using the set of variables $S_0 = |Q_0|^2 + 2|Q_1|^2$, $S_1 = |Q_0|^2 - 2|Q_1|^2$, $S_2 = i(Q_1Q_0^* - Q_0Q_1^*)$, and $S_3 = (Q_1Q_0^* + Q_0Q_1^*)$, Eq. (5) becomes

$$\begin{aligned} \frac{dS_1}{d\zeta} &= 4S_2, \\ \frac{dS_2}{d\zeta} &= \left(\frac{3}{2}S_0 + \delta_0 - \frac{1}{2}S_1 - 1\right)S_3 - 2S_1, \\ \frac{dS_3}{d\zeta} &= -\left(\frac{3}{2}S_0 + \delta_0 - \frac{1}{2}S_1 - 1\right)S_2. \end{aligned} \quad (6)$$

The quantity S_0 is a constant of the motion of Eq. (6) and, additionally, a second invariant is given by $S_1^2 + 2S_2^2 + 2S_3^2 = S_0^2$. We can find the solution of Eq. (6) with an integration scheme used to study the propagation of polarized light in birefringent Kerr waveguides [21]. Thus, we obtain

$$\begin{aligned} S_1(W) &= 4W + S_1(0), \\ S_3(W) &= W^2 + \left(\frac{1}{2}S_1(0) + 1 - \frac{3}{2}S_0 - \delta_0\right)W + S_3(0), \end{aligned} \quad (7)$$

where $W = \int_0^\zeta S_2(\tau) d\tau$. We use the second invariant to find the variable W , which is determined from an equation of motion for the conservative system $\frac{1}{2}(dW/d\zeta)^2 + V(W) = 0$, where $V(W) = \frac{1}{4}S_1^2 + \frac{1}{2}S_3^2 - \frac{1}{4}S_0^2$. Any trajectory in this potential starts at $\zeta = \zeta_0 = 0$ and $W = 0$ with $dW/d\zeta(\zeta_0 = 0) = S_2(0)$. Moreover, $dV(W=0)/dW = 2S_1(0) + S_3(0)[\frac{1}{2}S_1(0) + 1 - \frac{3}{2}S_0 - \delta_0]$ and $d^2V(W=0)/dW^2 = 8 + 2S_3(0) + [\frac{1}{2}S_1(0) + 1 - \frac{3}{2}S_0 - \delta_0^2]$. We choose a trajectory whose initial conditions coincide with a fixed point $[S_1(0), S_2(0), S_3(0)]$ of Eq. (6) when $\delta_0 = 0$. As a result, $dV(W=0)/dW = 2S_1(0) + S_3(0)[\frac{1}{2}S_1(0) + 1 - \frac{3}{2}S_0] = 0$. In addition, the assumption $|Q_0|^2 > 2|Q_1|^2$ at $\zeta = 0$ implies that $S_1(0) > 0$. Moreover, we suppose that Q_0 and Q_1 have the same phase at $\zeta = 0$. As a result, $S_3(0) > 0$ and $S_2(0) = 0$. Therefore, the positive sign of the second derivative $d^2V(W=0)/dW^2$ indicates that the fixed point $[S_1(0), S_2(0), S_3(0)]$ is an elliptic (equilibrium) point. A small value of $\delta_0 \neq 0$ with these initial conditions, according to the expression for the first derivative $dV(W=0)/dW = -\delta_0 S_3(0)$, induces a shift of the local minimum $V(W_{\min})$ either to the right or to the left of $W = 0$. As a result, when $\delta_0 \neq 0$, the trajectory starts at a turning point of the shifted potential $V(W)$ since $dW/d\zeta(\zeta_0 = 0) = 0$ and, therefore, the intensity oscillations are amplified.

To complete this qualitative explanation, we need to show that the variables $\theta_1 - \theta_{-1}$ and $|Q_1| - |Q_{-1}|$ are bounded and, therefore, stable. To this end, let us consider a

simplified model consisting of three waveguides Q_{-1} , Q_0 , and Q_1 , where $Q_{-1} \approx Q_1$. Using Eq. (3), the expression $Q_j = P_j \exp(-i\theta_j)$ and the approximation $|\theta_i - \theta_j| \ll 1$ for $i, j = -1, 0, 1$, we get the following equations for θ_j :

$$\frac{d\theta_j}{d\zeta} + 2P_j^2 + \left(\frac{P_{j-1}}{P_j} + \frac{P_{j+1}}{P_j}\right) = \delta_0 \delta_{0j}, \quad (8)$$

where $\delta_{00} = 1$ and $\delta_{0j} = 0$ for $j = \pm 1$. δ_0 stands for the defect. Taking into account the small order parameter of $|\theta_1 - \theta_{-1}| \ll 1$ and $|P_1 - P_{-1}| \ll P_{1,-1}$, we get the equations $d^2\Delta_{1,2}/d^2\zeta + \Omega\Delta_{1,2} = 0$, where $\Omega \equiv (2P_1 + P_0)(2/P_1 + P_0/P_1^2 - 4P_1)$, $\Delta_1 \equiv \theta_1 - \theta_{-1}$, $\Delta_2 \equiv P_1 - P_{-1}$. We have assumed that the variables P_n have a negligible variation since $|\delta_0| \ll 1$. The stability of these solutions is determined by $\Omega > 0$. Therefore, Δ_1 and Δ_2 are stable and do not depend on δ_0 . Thus, both the enhancement of the intensity oscillations and the boundedness of $\Delta_{1,2}$ suggest that R grows as δ_0 increases. This behavior agrees qualitatively with that of Fig. 3.

To further estimate the stability of our solutions, we have considered several random initial conditions in the interval $(P_n - \nu_{\max}, P_n + \nu_{\max})$ with $\nu_{\max} = 10^{-3}$, i.e., within a small neighborhood of $\theta_n = 0$. The P_n are given in Fig. 2. In this case, stable quasiperiodic evolution of $I_n(\zeta)$ has typically been found for distances as large as $\zeta \sim 10^5$ for $\delta_3 = 0.025$, $\delta_3 = 0.4$, and $\delta_3 = 1.25$. The calculated Liapunov exponents confirm that the dynamics in all these cases is quasiperiodic.

The modulus of the following complex order parameter measures the coherence of the system. This is defined as follows:

$$Z = \frac{\left| \sum_{j=1}^N \exp(-i\theta_j) \right|}{N}, \quad (9)$$

where N stands for the number of waveguides. This parameter was introduced by Kuramoto in the context of coupled phase oscillators [22,23]. If $Z = 1$, all the oscillators are in phase. When $Z = 0$, the phases θ_j are typically distributed uniformly between 0 and 2π . Z is an indicator of the temporal distribution of θ_j when these are either locked or unlocked. As shown below, frequent and large drops in Z are correlated with the presence of unlocked states. The center of mass ρ and the dispersion $\Delta\rho$ are defined as

$$\begin{aligned} \rho &= \frac{\sum_{j=1}^N jI_j}{\sum_{j=1}^N I_j}, \\ (\Delta\rho)^2 &= \frac{\sum_{j=1}^N j^2I_j}{\sum_{j=1}^N I_j} - \rho^2. \end{aligned} \quad (10)$$

These last two quantities have been used in the context of BEC [13] as well as in the theory of one-dimensional propagation of quasiparticles, such as electrons and excitons [24].

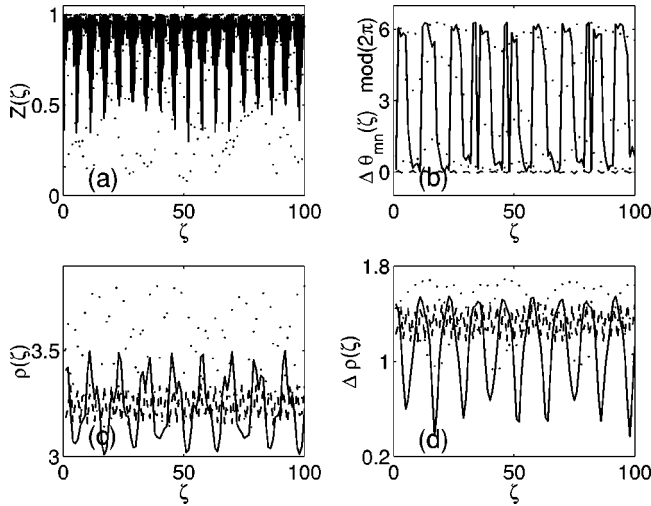


FIG. 4. (a) Plot of $Z(\zeta)$ versus distance ζ . (b) Plot of the largest phase difference $\Delta\theta_{mn}(\zeta)$ versus distance ζ . (c) Plot of $\rho(\zeta)$ versus distance ζ . (d) Plot of $\Delta\rho(\zeta)$ versus distance ζ . Here, $\delta_3=0.4$ (solid line), $\delta_3=0.025$ (dashed line), and $\delta_3=1.25$ (dotted line).

ρ and $\Delta\rho$ describe the level of localization of the intensity in the array, which takes place when $\delta_3 > 0$, as shown below. In the case when there are no phase slips in the relative phases across the waveguides $\Delta\theta_{mn} = \theta_m - \theta_n$, the order parameter $Z \approx 1$. This is illustrated in the dashed lines of Figs. 4(a) and 4(b), where $Z \approx 1$ for $\delta_3 = 0.025$. However, as shown also in Figs. 4(a), 4(b), Z drops substantially below 1 since at least one of the $\Delta\theta_{mn}$ is unlocked when $\delta_3 = 0.4$ or $\delta_3 = 1.25$. In the context of the aforementioned BEC models, the phase locking of $\Delta\theta_{mn}$ is associated with the superfluid regime. However, when $\Delta\theta_{mn}$ is unbounded, the system is said to behave as an insulator [13]. Moreover, the center of mass ρ oscillates near the position of the central waveguide, which, as seen in Fig. 2(a), has the largest intensity. Figures 4(c) and 4(d) suggest that the oscillations of I_n are localized within a small neighborhood. Typically, the presence of a defect $\delta_3 > 0$, even in the chaotic regime as we will see in the next section, produces oscillations of ρ whose mobility is highly inhibited. This contrasts with the Anderson localization phenomenon, where the presence of uncorrelated disorder is necessary to inhibit the quasiparticle propagation [24].

V. CHAOTIC SOLUTIONS

Let us study the array consisting of seven waveguides in an interval of the defect δ_3 , where it is possible to induce Hamiltonian chaos. As shown below, a suitable defect induces a bifurcation which triggers the onset of chaotic behavior. In other words, this defect perturbs a periodic orbit, setting up a typical scenario for Hamiltonian chaos [18]. That is, several resonance surfaces in the system overlap generating stochastic regions in phase space. Since the number of degrees of freedom of the system is larger than two, the generated stochastic regions form an intricate web in phase space known as the Arnold web [18]. As before, $\delta_3 = 0$ for $n \neq 3$ and the initial conditions are those of the previous section. In contrast to the quasiperiodic case, where $I_1 \approx I_5$, I_2

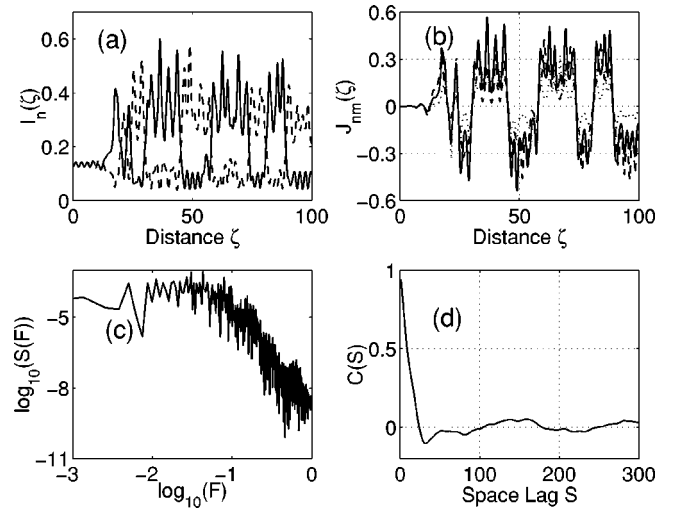


FIG. 5. (a) Plot of the intensities I_1 (solid line) and I_5 (dashed line) versus ζ . (b) Plot of J_{15} (solid line), J_{24} (dashed line), J_{76} (dotted line) versus ζ . (c) Plot of $\log_{10}S(F)$ versus $\log_{10}(F)$ for $I_3(\zeta)$. (d) Plot of the ACF $C(\tau)$ of $K_{15}(\zeta)$. The autocorrelation functions $C(\tau)$ for K_{15} , K_{24} , and K_{76} coincide exceptionally well. Here $\delta_3 = -0.00785$.

$\approx I_4$, and $I_6 \approx I_7$ as shown in Fig. 3, the onset of chaos is manifested via a symmetry breaking of these intensity pairs. The existence of at least a single positive Liapunov exponent in the chaotic regime implies divergence of nearby trajectories [18]. This divergence explains why two otherwise intensity correlated waveguides, such as (I_1, I_5) , lose their relative symmetry when chaos arises. Indeed, the onset of chaos in Hamiltonian systems is associated with the destruction of integrals of motion [18], which, in turn, destroy the symmetries in the system. This symmetry breaking is shown in Fig. 5(a), where each of the aforementioned intensity pairs executes initially stable small amplitude oscillations before displaying erratic behavior. This behavior is similar to that near the coupling resonance in the three-dimensional billiards problem, where a particle bounces back and forth between a smooth and a periodically rippled wall [18].

In the chaotic regime and provided that $\delta_3 < 0$, in spite of the symmetry breaking of the aforementioned intensity pairs, a very interesting form of synchronization can take place between certain signals emerging from different pairs of waveguides. To this end, let us define the variables $J_{15} = I_1 - I_5$, $J_{24} = I_2 - I_4$, and $J_{76} = I_7 - I_6$. Our simulations show that J_{15} , J_{24} , and J_{76} have the same sign during most of the time. This is clearly appreciated in Fig. 5(b). That is, in spite of the chaotic state, when $J_{15} > 0$ (< 0), it follows almost simultaneously that $J_{24} > 0$ (< 0) and $J_{76} > 0$ (< 0). This behavior holds for lengths as large as $\zeta \sim 10^5$. We would like to know if this coherent behavior of the signals J_{mn} suggests some kind of synchronization. The answer is affirmative from the point of view of synchronization of symbolic information (SSI) [14,15]. According to this notion, two arbitrary oscillators are perfectly synchronized in an information sense if they produce the same information, i.e., symbols generated by one system map one-to-one to symbols emitted by the other system. Strictly speaking, this form of synchronization

requires that the common information be emitted at precisely the same time. This concept was used to experimentally demonstrate that synchronization of information is possible in an electronic oscillator circuit driven by a logistic map [15]. In Ref. [15], the chaotic signals of both systems are compared using their symbolic dynamics. In our case, Fig. 5(b) suggests that the signals J_{15} , J_{24} , and J_{76} exhibit equivalent information at the same average rate. This, however, does not contradict the fact that the usual notion of synchronization cannot be applied to Hamiltonian systems, such as ours, since volume has to be preserved in phase space. Indeed, the trajectories of coupled systems have to collapse to the synchronization manifold [25], which is only possible in dissipative systems. In our system, instead, we compare the chaotic signals J_{nm} using just their symbolic dynamics, i.e., we only consider the sign of J_{mn} .

The signals I_j , where $j=1, \dots, 7$, are chaotic. Indeed, the broadband power spectrum $S(F)$ of I_3 , shown in Fig. 5(c), where F is the normalized frequency, indicates the presence of chaotic behavior. In this figure, $\delta_3 = -0.00785$. To generate a symbolic sequence out from J_{15} , J_{24} , and J_{76} , we replace the value of J_{ij} by “-1” or “1” provided that $J_{ij} < 0$ or $J_{ij} > 0$, respectively. Let us call these new signals K_{ij} . In addition, the symmetry of the system indicates that $\langle J_{ij} \rangle = \langle K_{ij} \rangle = 0$, where $\langle \cdot \rangle$ stands for the sample average. We have calculated the autocorrelation function (ACF) $C(S)$ for these signals, where

$$C(S) = \frac{\sum_{t=1}^{t=M-S} (H_t - \langle H \rangle)(H_{t+S} - \langle H \rangle)}{\sum_{t=1}^{t=M} (H_t - \langle H \rangle)^2}.$$

In this equation, S is the space lag, M is the number of data, and $\langle \cdot \cdot \rangle$ stands for sample average [18]. It is well known that a fast decay of $C(S)$ suggests the presence of chaotic behavior [18]. The ACF $C(S)$ of K_{15} , K_{24} , and K_{76} coincide exceptionally well for all space lags S considered. Indeed, all of them collapse to the solid line of Fig. 5(d) for which $\delta_3 = -0.00785$. In contrast, the ACF $C(S)$ of J_{15} , J_{24} , and J_{76} agree only at a qualitative level. As expected, the first zero of these ACF occurs at the same space lag S , since these signals change sign almost simultaneously. Moreover, we make use of the linear cross correlation function R for a given pair of signals K_{mn} and K_{ij} in order to quantify the extent of SSI. If $R=1$, the signal pair is fully correlated and SSI is perfect. For the sake of precision, we define R as the minimum cross correlation of the signal pairs (K_{15}, K_{24}) , (K_{15}, K_{76}) , and (K_{24}, K_{76}) . After considering several chaotic signals whose length is $\zeta \sim 10^5$ for different values of δ_3 , we obtained the following values for R : $R \approx 0.242$ for $\delta_3 = 0.25$, $R \approx 0.506$ for $\delta_3 = 0.075$, $R \approx 0.668$ for $\delta_3 = 0.0575$, $R \approx 0.987$ for $\delta_3 = -0.00785$, $R \approx 0.972$ for $\delta_3 = -0.01575$, $R \approx 0.825$ for $\delta_3 = -0.25$, and $R \approx 0.417$ for $\delta_3 = -1.5$.

It is remarkable how the chaotic synchronization of symbolic information (SSI) of J_{mn} is manifested in the dynamics of $\Delta_{mn} = \theta_m - \theta_n$ when $\delta_3 < 0$. Indeed, as suggested by Fig. 6(b), all the Δ_{mn} are bounded when SSI occurs, i.e., when

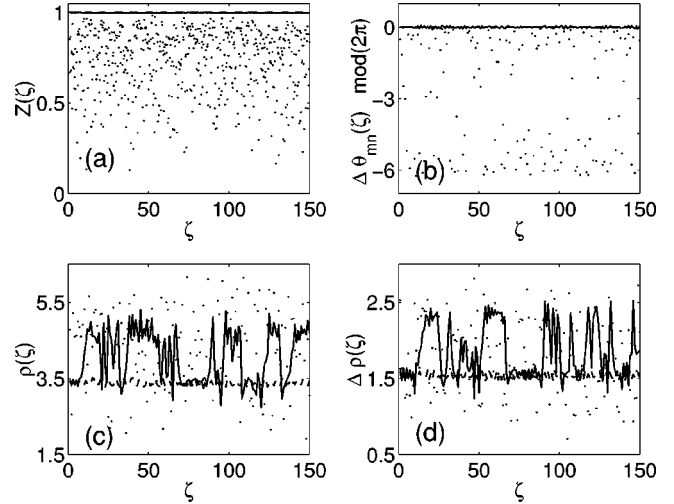


FIG. 6. Same as Fig. 4 but for the following parameters. $\delta_3 = -0.00785$ (solid line), $\delta_3 = -0.005$ (dashed line), and $\delta_3 = -1.5$ (dotted line).

$R \approx 1$. This was found for $\delta_3 = -0.005$, $\delta_3 = -0.00785$, and $\delta_3 = -0.01575$. This locking of phases θ_m and θ_n is also referred to as phase synchronization [26]. The latter has been extensively studied in the context of coupled self-sustained chaotic oscillators [26]. However, the presence of phase synchronization does not imply the observation of SSI. An example is the case $\delta_3 = 0.075 > 0$ for which $R \approx 0.506$. Moreover, when $\delta_3 < 0$ and the onset of phase slips of Δ_{mn} occurs, degradation of SSI takes place. The case $\delta_3 = -1.5$, for which $R \approx 0.417$, illustrates this situation in Fig. 6(b). Figures 6(a) and 6(b) indicate that when SSI ($R \approx 1$) occurs, the order parameter $Z \approx 1$. However, as shown in these two figures, when phase slips of Δ_{mn} arise, both Z and the cross correlation R drop below 1. Moreover, when $\delta_3 > 0$ and in the presence of phase locking, $Z \approx 1$ and R is typically far below 1. This means that while the phases θ_m are locked, the signals J_{mn} do not synchronize in the information sense. This is illustrated in Figs. 7(a) and 7(b) for which $\delta_3 = 0.075$ and $\delta_3 = 0.0575$, respectively. The associated values of R are written above. When $\delta_3 > 0$, the onset of phase slips signals the lack of coherence and both Z and R become smaller than 1.

Figures 6(c), 6(d) and Figs. 7(c), 7(d) suggest that in the chaotic regime, the center of mass ρ fluctuates near the position of the central waveguide provided that $\delta_3 > \delta_3^{(c)}$, where $\delta_3^{(c)} < 0$ and $|\delta_3^{(c)}| \ll 1$. Therefore, when $\delta_3 > 0$, ρ is typically localized. This contrasts with the case $\delta_3 < \delta_3^{(c)} < 0$, as seen in Figs. 6(c), 6(d), where ρ executes large amplitude oscillations. To gain further insight, let us consider Fig. 8. In Fig. 8(a), for which $\delta_3 = -0.00785$, the minima and maxima of I_n are roughly the same. However, provided that $\delta_3 > 0$, Figs. 8(b), 8(c), and 8(d) suggest that the following inequalities hold: $I_3 > I_2$, $I_3 > I_4$, $\langle I_2 \rangle \approx \langle I_4 \rangle$ and $\langle I_{2,4} \rangle > \langle I_i \rangle$ for $i=1,5,6,7$. $\langle \cdot \cdot \rangle$ stands for sample average. The latter does not depend on whether the oscillators are either chaotic or quasiperiodic, phase locked or unlocked.

To further characterize the DNLSE dynamics, let us consider the spectrum of Liapunov exponents Λ_n . The DNLSE

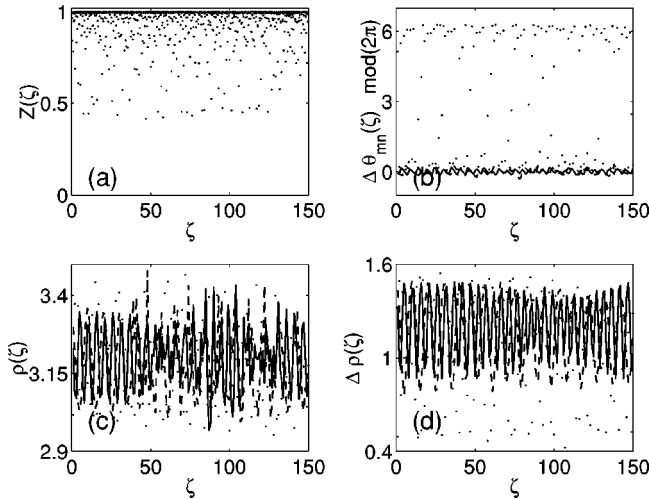


FIG. 7. Same as Fig. 4 but for the following parameters. $\delta_3 = 0.0575$ (solid line), $\delta_3 = 0.075$ (dashed line), and $\delta_3 = 0.25$ (dotted line).

has two constants of motion, namely, the norm and the Hamiltonian. Moreover, the DNLSE is an autonomous flow. The above features along with the symmetry of the Liapunov exponents of Hamiltonian systems [18], suggests that at least four Liapunov exponents are equal to zero. In the chaotic regime these Liapunov spectra are shown in Figs. 9(a)–9(c). When SSI takes place, there is a single positive Liapunov exponent whose magnitude is much larger than that of the other positive exponents. The latter is appreciated in Fig. 9(a). When $\delta_3 < 0$ and phase slips of Δ_{mn} occur, typically, the nonvanishing Liapunov exponents Λ_n have roughly the same order of magnitude as shown in Fig. 9(b). A similar picture arises when $\delta_3 > 0$, the dynamics is chaotic and phase slips occur. This is shown in Fig. 9(c). To characterize the statistics of the signals K_{ij} when SSI takes place, let us consider the dependence of the probability density function (PDF) on the length L of the “−1” and “1” intervals for

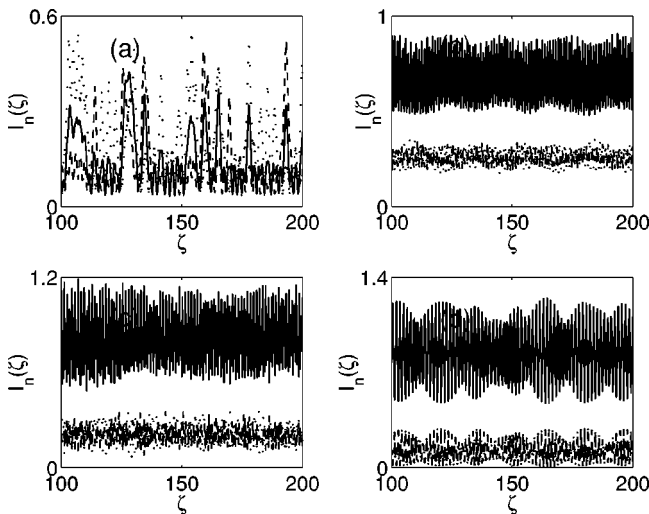


FIG. 8. Plot of the intensities I_3 (solid line), I_2 (dashed line), and I_4 (dotted line) versus ζ for (a) $\delta_3 = -0.00785$, (b) $\delta_3 = 0.075$, (c) $\delta_3 = 0.25$, and (d) $\delta_3 = 1.25$.

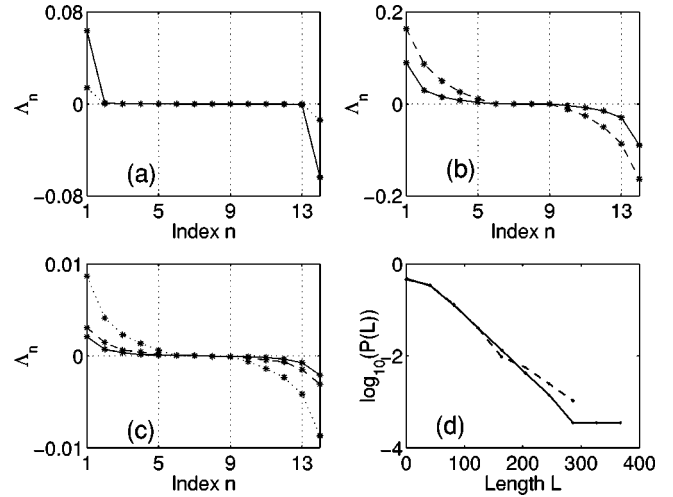


FIG. 9. Plot of the Liapunov exponents Λ_n versus index n . (a) $\delta_3 = -0.005$ (dotted line), $\delta_3 = -0.00785$ (solid line). Here SSI takes place, i.e., $R \approx 1$. (b) $\delta_3 = -0.25$ (solid line), $\delta_3 = -1.5$ (dashed line). (c) $\delta_3 = 0.0575$ (solid line), $\delta_3 = 0.075$ (dashed line), $\delta_3 = 0.25$ (dotted line). (d) $\log_{10}[P(L)]$ versus L for $\delta_3 = -0.00785$ for the “−1” intervals L (solid line) and “1” intervals L (dashed line).

$\delta_3 = -0.00785$. By symmetry arguments, the PDF $P(L)$ of these intervals are the same. This is suggested by Fig. 9(d), which shows that the core of $P(L)$ has to a good extent an exponential decay, where the solid and dashed lines stand for the “−1” and “1” intervals, respectively. However, the signals K_{ij} have nonzero memory as indicated by the ACF $C(S)$ of Fig. 5(d).

We have carried out a continuation study of the stationary solutions for the case with seven and six waveguides. It was found in both cases that the continued stationary solution remains stable as the defect parameter δ_3 is changed from $\delta_3 = 0$ to the first bifurcation. In this bifurcation at $\delta_3 = \delta_3^B$, two eigenvalues leave the unit circle at the point $(1, 0)$, i.e., in a tangent bifurcation. The period of the stationary solutions along the bifurcation branch remains constant. Past this bifurcation point, the continued stationary solution becomes unstable. This is shown in Fig. 10, where the amplitude of the stationary solution is plotted against δ_3 . In the neighborhood of the stable stationary solution, just before the bifurcation, the dynamics is quasiperiodic. Instead, just after the bifurcation point, initial conditions in the vicinity of the unstable stationary solution trigger the onset of the SSI dynamics.

VI. NONLINEAR BIREFRINGENCE EFFECTS

We can generalize our model to consider the case when the two orthogonally polarized states of the electric field in each waveguide interact with those of the nearest-neighbor waveguides through the evanescent fields [27]. In a given waveguide, however, we assume that light propagates in an elliptically birefringent medium. A recent experiment has reported the first observation of discrete vector solitons in waveguide arrays of $\text{Al}_x\text{Ga}_{1-x}\text{As}$ [10]. Using the same as-

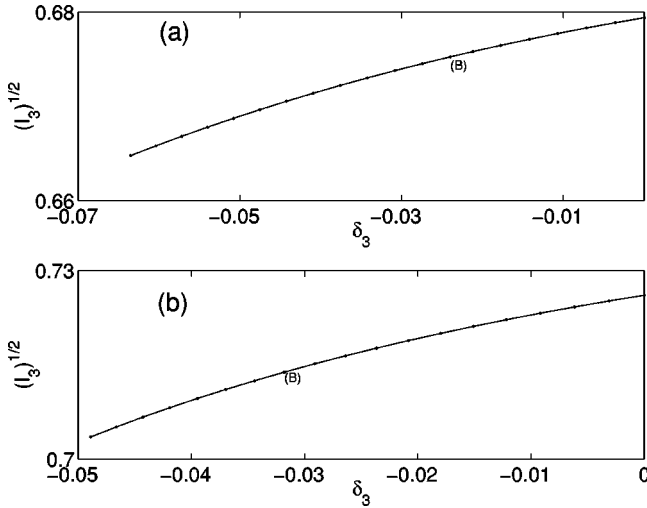


FIG. 10. Plot of the amplitude $(I_3)^{1/2}$ of the stationary state versus $\delta_3 < 0$ for (a) $N=7$ and (b) $N=6$. This is a numerical continuation of the stationary solutions of Fig. 2. The label (B) stands for the bifurcation point.

sumptions of Sec. II, this system can be modeled with the following set of equations [27,28]:

$$\begin{aligned}
 i \frac{\partial Q_n^x}{\partial \zeta} + \delta_n^x Q_n^x + (Q_{n-1}^x + Q_{n+1}^x - 2Q_n^x) \\
 + 2(|Q_n^x|^2 + B|Q_n^y|^2)Q_n^x = 0, \\
 i \frac{\partial Q_n^y}{\partial \zeta} + \delta_n^y Q_n^y + (Q_{n-1}^y + Q_{n+1}^y - 2Q_n^y) \\
 + 2(|Q_n^y|^2 + B|Q_n^x|^2)Q_n^y = 0,
 \end{aligned} \quad (11)$$

where the superindexes x and y stand for the two orthogonally polarized states of light. The parameter B models the nonlinear birefringence factor, where $\frac{2}{3} < B < 2$ [27]. The other labels have the same meaning as those of Sec. II. The defect parameters are given by $\delta_n^{x,y} = (\beta_n^{x,y} - \beta_n^{x,y})/C$. $\beta_n^{x,y}$ are suitable constants. We will assume that the propagation constant difference $\beta_n^x - \beta_n^y$ is large enough. Moreover, $\beta_n^x = \beta_m^x$ and $\beta_n^y = \beta_m^y$ for all n and m with the exception of the central waveguide for which $n=3$. A large enough $|\beta_n^x - \beta_n^y|$ is required to neglect nonlinear terms which undergo spatial modulation with the frequency $|\beta_n^x - \beta_n^y|$ [27].

The associated equations for the stationary states of $Q_n^{x,y} = P_n^{x,y} \exp(-i\theta_n^{x,y})$, where $I_n^{x,y} = |Q_n^{x,y}|^2$, are written below following the lines of Sec. III. We set $dP_n^{x,y}/d\zeta = 0$ and $\theta_n^{x,y} = \theta_m^{x,y}$. As before, we define the parameters $d\theta_n^{x,y}/d\zeta = \lambda^{x,y}$. Hence, from Eq. (11) we obtain the following map:

$$\begin{aligned}
 X_{n+1} &= P_n^x, \\
 P_{n+1}^x &= \{\Gamma_n^x - 2[(P_n^x)^2 + B(P_n^y)^2]\}P_n^x - X_n, \\
 Y_{n+1} &= P_n^y,
 \end{aligned}$$

$$P_{n+1}^y = \{\Gamma_n^y - 2[(P_n^y)^2 + B(P_n^x)^2]\}P_n^y - Y_n, \quad (12)$$

where $\Gamma_n^{x,y} = 2 - \lambda^{x,y} - \delta_n^{x,y}$. The Jacobian J of this map is area preserving, i.e., $J=1$. In Eq. (12), we will consider the case where $\lambda^x = \lambda^y = \lambda$ and $\delta_n^{x,y} = 0$. The fixed points of this map satisfy $X_n = P_n^x$ and $Y_n = P_n^y$. These are the following: $\Pi_1 = (X_n, P_n^x, Y_n, P_n^y) = (0, 0, 0, 0)$, $\Pi_2 = (0, 0, \pm \sqrt{-\lambda/2}, \pm \sqrt{-\lambda/2})$, $\Pi_3 = (\pm \sqrt{-\lambda/2}, \pm \sqrt{-\lambda/2}, 0, 0)$, $\Pi_4 = (\pm \sqrt{-\lambda/2}/\sqrt{1+B}, \pm \sqrt{-\lambda/2}/\sqrt{1+B}, \pm \sqrt{-\lambda/2}/\sqrt{1+B}, \pm \sqrt{-\lambda/2}/\sqrt{1+B})$, and $\Pi_5 = (\pm \sqrt{-\lambda/2}/\sqrt{1+B}, \pm \sqrt{-\lambda/2}/\sqrt{1+B}, \mp \sqrt{-\lambda/2}/\sqrt{1+B}, \mp \sqrt{-\lambda/2}/\sqrt{1+B})$. The eigenvalues of these fixed points are the following. For the point Π_1 , the eigenvalues are $1 - \lambda/2 \pm \sqrt{\lambda^2 - 4\lambda/2}$ with multiplicity 2. For the points $\Pi_{2,3}$ these are $1 + \lambda \pm \sqrt{\lambda^2 + 2\lambda}$ and $1 - \lambda/2 + B\lambda/2 \pm \sqrt{\lambda^2(B-1)^2 + 4\lambda(B-1)}/2$. Finally for the points $\Pi_{4,5}$, the eigenvalues are $1 + \lambda \pm \sqrt{\lambda^2 + 2\lambda}$ and $1 + B + \lambda(1 - B) \pm \sqrt{\lambda^2(B-1)^2 + 2\lambda(1-B^2)}/(1+B)$.

We look for fixed points, such as $\Pi_{4,5}$, where $X_n = \pm Y_n$ and such that the corresponding eigenvalues are complex conjugates. This simplifies Eq. (12) and a Hamiltonian map on the plane is obtained. As in Sec. III, we find suitable resonances in this map, which, in turn, will become the amplitudes of the stationary solutions of Eq. (11). We choose to consider the case for which $B = \frac{2}{3}$. At the fixed points Π_4 and Π_5 where $B > 1$, there is no interval for λ where all the eigenvalues are complex numbers. Instead, in the case $B = \frac{2}{3}$, the complex eigenvalues suggest the presence of resonance islands around $\Pi_{4,5}$. Indeed, for $B = \frac{2}{3}$, the eigenvalues are $1 + \lambda \pm \sqrt{\lambda^2 + 2\lambda}$, $1 + \lambda/5 \pm \sqrt{\lambda^2 + 10\lambda/5}$ and therefore, in the interval $-2 < \lambda < 0$, we find complex conjugate eigenvalues.

Now we will consider the case where the stationary solutions are determined by the resonance of period 7, which is localized around $\Pi_{4,5}$. The case with the period 6 resonance can be treated similarly. The dependence of the amplitudes P_n on the parameter B is shown in Fig. 11(a). As the parameter B increases, in general, the magnitude of these amplitudes decrease while keeping a similar profile. The structure of the phase space (P_n, P_{n+1}) for $0 < B < 1$ is similar to that of Fig. 1(a). Our numerical simulations indicate that these stationary solutions are stable.

Let us consider initial conditions in a small vicinity of the stationary solutions and a small positive defect $0 < \delta_3^{x,y} \ll 1$. In this interval, the solutions are quasiperiodic. As the positive defect $\delta_3^{x,y}$ becomes larger, the symmetric pairs of waveguides, such as $I_1^{x,y} I_5^{x,y}$, increase their intensity correlations. That is precisely what we show in Fig. 11(b). That is, as in Sec. IV, the oscillation amplitudes of $I_n^{x,y}$ increase, while the intensity difference between symmetric waveguides remains the same on average. In particular, $I_1^x \approx I_1^y \approx I_5^x \approx I_5^y$ as $\delta_3^{x,y} > 0$ becomes larger. These induced correlations are robust with respect to small differences between δ_3^x and δ_3^y .

It is also possible to induce Hamiltonian chaos in this system. For a suitable $\delta_3^{x,y}$ in an interval $-1 \ll \delta_3^{x,y} < 0$, where $\delta_n^{x,y} = 0$ for $n \neq 3$, SSI can take place. However, I_n^x diverges from its otherwise symmetric waveguide, in particu-

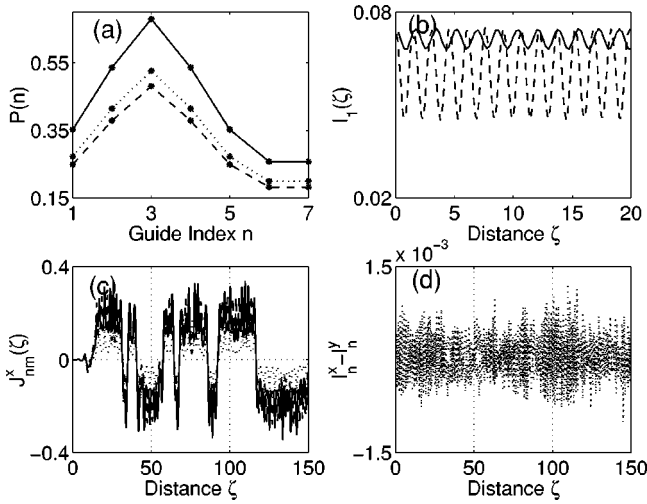


FIG. 11. Case with seven waveguides and $\Gamma=2.5$. (a) Plot of the stationary fields P_n versus waveguide index for $B=0$ (solid line), $B=0.5$ (dotted line), and $B=1$ (dashed line). (b) Plot of $I_1^x(\zeta)$ when $B=0.5$. $\delta_3^{x,y}=0.005$ (solid line), $\delta_3^{x,y}=0.025$ (dashed line). (c) Plot of J_{15}^x (solid line), J_{24}^x (dashed line), J_{76}^x (dotted line) versus ζ for $\delta_3^{x,y}=-0.00785$. (d) Plot of $I_1^x-I_1^y$, $I_2^x-I_2^y$, and $I_3^x-I_3^y$ versus ζ for $\delta_3^{x,y}=-0.00785$.

lar, I_1^x diverges from I_5^x . The picture is similar to that of Sec. V. When the initial conditions are in the neighborhood of the stationary solution of Fig. 11(a) and when the defects are $\delta_3^x = \delta_3^y = -0.00785$, the set of signals $J_{15}^{x,y} = I_1^{x,y} - I_5^{x,y}$, $J_{24}^{x,y} = I_2^{x,y} - I_4^{x,y}$, and $J_{76}^{x,y} = I_7^{x,y} - I_6^{x,y}$ synchronize in the information sense. This is what we observe in Fig. 11(c) for the variables J_{15}^x , J_{24}^x , and J_{76}^x . Moreover, the differences $I_n^x - I_n^y$ remain bounded for all n as shown in Fig. 11(d).

VII. CONCLUSIONS AND DISCUSSION

We have studied the intensity correlations of electromagnetic fields that arise in certain pairs of coupled Kerr waveguides, i.e., oscillators, when the system dynamics is quasiperiodic or chaotic. These correlations are generated by a new family of solutions of the DNLSE, which has as initial conditions the neighborhood of a set of stationary solutions $Q_n(\zeta) = P_n \exp(-i\lambda\zeta)$ with real-valued time-independent amplitudes P_n and an oscillation frequency λ . The P_n , in turn, are given by the resonances of a suitable Hamiltonian map. Our solutions differ from the breather solutions [6,16,17], which are obtained from the same area-preserving map, in some important features. First, the homoclinic (heteroclinic) orbits of the Hamiltonian map give rise to the breathers, known also as bright (dark) DSS, while the map resonances determine our stationary solutions. Second, the breathers require, at least formally, an infinite number of waveguides, while our stationary solutions need only a finite number of waveguides M , where M is determined by the periodicity of the resonance under consideration. Our stationary solutions satisfy periodic boundary conditions and have the same phase. The second and third properties make our solutions different from those studied by Johansson *et al.* [20].

When the initial conditions are close to the stationary solutions, a positive defect ($\delta_3 > 0$) can induce a substantial amplification of the quasiperiodic intensity oscillations. In addition, certain pairs of waveguides show intensity correlations that become stronger as the positive defect becomes larger. We have shown analytically, in models consisting of a few waveguides, that the aforementioned intensity correlations take place. Chaos emerges via a symmetry breaking instability of the aforementioned intensity pairs for a small negative defect ($\delta_3 < 0$). In this case, a very interesting form of synchronization takes place between certain signals generated by different pairs of waveguides. These signals synchronize in the information sense, since their binary symbolic dynamics coincide with an excellent accuracy. Thus, we provide an example where synchronization, in the information sense, is possible in a Hamiltonian system. For arbitrary initial conditions and defects δ_3 , typically, synchronization of symbolic information (SSI) does not take place. Moreover, we have carried out a continuation study of the stationary solutions. We found that along the stationary solution branch there is a bifurcation which triggers the onset of the SSI dynamics.

We have used the linear cross correlation function R to quantify the extent of SSI. In the presence of phase synchronization of the waveguides, the coherence function Z , which was introduced by Kuramoto [22], is typically close to its maximum, i.e., $Z \sim 1$. In contrast, the presence of phase slips across the oscillators destroys the aforementioned coherence. Typically, the nonvanishing Liapunov exponents have the same order of magnitude. However, when SSI takes place, phase synchronization of all oscillators follows with $Z \approx 1$ and roughly a single positive Liapunov exponent is present. When $\delta_3 > 0$, the center of mass, i.e., the average position of the intensities, executes small amplitude oscillations in both the chaotic or nonchaotic regimes. That is, the waveguide intensities have relatively small fluctuations and, on average, a persistent localized pattern of intensities is observed. In contrast, when $\delta_3 < 0$, this center of mass typically executes large amplitude oscillations in the chaotic regime. We have also calculated the probability density function (PDF) of the length of an interval with a given binary symbol. The core of these PDF has an exponential form when SSI takes place. We have also studied a generalization of the DNLSE to consider arrays of elliptically birefringent waveguides. In this system, the quasiperiodic and chaotic dynamics is qualitatively similar to that of the DNLSE.

The present study can be extended to consider other types of coupled nonlinear waveguides, such as quadratic waveguides. Finally, we point out that our solutions may describe interesting effects in quasi-1D Bose-Einstein condensates (BEC's) confined in periodic potentials [13], since the latter has been modeled, in the tight binding approximation, with the DNLSE [13].

ACKNOWLEDGMENTS

This work was also supported by CONACYT-México.

- [1] D.N. Christodoulides and R.I. Joseph, *Opt. Lett.* **13**, 794 (1988).
- [2] A.B. Aceves, C. de Angelis, T. Peschel, R. Muschall, F. Lederer, S. Trillo, and S. Wabnitz, *Phys. Rev. E* **53**, 1172 (1996).
- [3] H.S. Eisenberg, Y. Silberberg, R. Morandotti, A.R. Boyd, and J.S. Aitchison, *Phys. Rev. Lett.* **81**, 3383 (1998).
- [4] R. Morandotti, U. Peschel, J.S. Aitchison, H.S. Eisenberg, and Y. Silberberg, *Phys. Rev. Lett.* **83**, 2727 (1999).
- [5] H.S. Eisenberg, R. Morandotti, Y. Silberberg, J.M. Arnold, G. Pinnelli, and J.S. Aitchison, *J. Opt. Soc. Am. B* **19**, 2938 (2002).
- [6] S. Flach and C.R. Willis, *Phys. Rep., Phys. Lett.* **295C**, 182 (1998).
- [7] P.G. Kevrekidis, K.O. Rasmussen, and A.R. Bishop, *Int. J. Mod. Phys.* **15**, 2833 (2001); M. Johansson and S. Aubry, *Nonlinearity* **10**, 1151 (1997).
- [8] A.S. Davydov, *Phys. Scr.* **20**, 378 (1978).
- [9] B. Denardo *et al.*, *Phys. Rev. Lett.* **68**, 1730 (1992).
- [10] J. Meier, G.I. Stegeman, H.S. Eisenberg, Y. Silberberg, R. Morandotti, and J.S. Aitchison (unpublished).
- [11] U. Peschel, R. Morandotti, J.S. Aitchison, H.S. Eisenberg, and Y. Silberberg, *Appl. Phys. Lett.* **75**, 1348 (1999).
- [12] M.J. Ablowitz and Z.H. Musslimani, *Phys. Rev. Lett.* **87**, 254102 (2001).
- [13] R. Carretero-González and K. Promislow, e-print cond-mat/0105600; J.C. Bronski *et al.*, *Phys. Rev. E* **64**, 056615 (2001); A. Trombettoni, A. Smerzi, and A.R. Bishop, *Phys. Rev. Lett.* **88**, 173902 (2002).
- [14] A. Shabunin, V. Demidov, V. Astakhov, and V. Anishchenko, *Phys. Rev. E* **65**, 056215 (2002); M. Palus, V. Komarek, Z. Hrnčir, and K. Sterbova, *ibid.* **63**, 046211 (2001).
- [15] N.J. Corron, S.D. Pethel, and K. Myneni, *Phys. Rev. E* **66**, 036204 (2002).
- [16] D. Hennig and H. Gabriel, *Phys. Rev. E* **57**, 2371 (1998); D. Hennig, K. Rasmussen, H. Gabriel, and A. Bülow, *ibid.* **54**, 5788 (1996).
- [17] T. Bountis, H.W. Capel, M. Kollmann, J.C. Ross, J.M. Bergamin, and J.P. van der Weele, *Phys. Lett. A* **268**, 50 (2000).
- [18] A.J. Lichtenberg and M.A. Lieberman, *Regular and Stochastic Motion* (Springer Verlag, Berlin, 1993).
- [19] C.L. Pando L., *Phys. Lett. A* **309**, 68 (2003).
- [20] M. Johansson *et al.*, *Eur. Phys. J. B* **29**, 279 (2002); A.M. Morgante *et al.*, *Phys. Rev. Lett.* **85**, 550 (2000); A.M. Morgante *et al.*, *Physica D* **162**, 53 (2002).
- [21] C.L. Pando L., *Phys. Rev. A* **45**, 5311 (1992).
- [22] Y. Kuramoto, *Chemical Oscillations, Waves and Turbulence* (Springer Verlag, Berlin, 1984).
- [23] C.L. Pando L., *Phys. Lett. A* **273**, 70 (2000).
- [24] D. Hennig and G.P. Tsironis, *Phys. Rep.* **307**, 334 (1999).
- [25] N.F. Rulkov, M.M. Sushchik, L.S. Tsimring, and H.D.I. Abarbanel, *Phys. Rev. E* **51**, 980 (1995).
- [26] A. Pikovsky, M. Rosenblum, and J. Kurths, *Synchronization: A Universal Concept in Nonlinear Sciences* (Cambridge University Press, Cambridge, 2001).
- [27] G.P. Agrawal, *Nonlinear Fiber Optics* (Academic Press, San Diego, 1995).
- [28] M.J. Ablowitz and Z.H. Musslimani, *Phys. Rev. E* **65**, 056618 (2002).